ISBN: 978-3-95450-225-7 ISSN: 2673-5571 doi:10.18429/JACoW-HB2021-MOP21

3D SYMPLECTIC SPACE CHARGE IMPLEMENTATION IN THE LATEST MAD-X VERSION

A. Latina, F. Schmidt, H. Renshall, CERN, Geneva, Switzerland,
Y. Alexahin, FNAL, Batavia, USA

Abstract

In 2018 as part of a collaboration between CERN and FNAL, the space charge (SC) implementation has been upgraded in a test version of MAD-X. The goal has been to implement the 3D symplectic SC kick together with a number of new features and benchmark it with earlier MADX-SC versions. Emphasis was given to the use of the Sigma Matrix approach that allows to extend MAD-X optics calculations.

In the meantime, significant effort has been made to fully debug and optimize the code and in particular to achieve a speed-up of the simulations by a factor of 2. The code has been ported to the latest MAD-X version, the elaborated set-up procedures have been automated and a user manual has been written.

INTRODUCTION

In 2010 (see Ref. [1]) V. Kapin and Y. Alexahin from FNAL started to implement the frozen space charge model into MAD-X [2]. One of the authors, F. Schmidt, joined their effort in 2012, establishing a special Fermilab version that we call MADX-SC, that has been presented in Ref. [3]. In the meantime, we have made a thorough cleaning and debugging of the code and have ported it to the latest MAD-X version. A manual has also been provided [4].

MADX-SC features both the frozen SC mode (as requested by BNL [5]) and the adaptive SC mode, the latter means that the SC force is recalculated when the emittances or beam intensity are changing. One can consider this as somewhere in between frozen and the full self-consistent mode, the latter provided in SC Particle-In-Cell (PIC) codes like Py-Orbit [6]. The adaptive mode allows for SC simulations with a few 1,000 macro-particles, and is therefore very fast and the only way to reach long periods, e.g., 500,000 turns for typical CERN PS SC runs. However, these SC force recalculations introduce some noise to the beam that needs to be minimized by increasing the number of macro-particles. For the PS simulation we had to increase the number of macro-particles from 1,000 to 2,000 to reduce the noise to an acceptable level. Nevertheless, this has to be seen as a compromise between simulation speed and artificial emittance growth due to numerical noise, although this is much less of a problem than for the PIC simulations.

This report discusses the physics aspects of MADX-SC in the first chapter, and summarizes the latest code development in the second chapter.

THE PHYSICS OF THE MADX-SC IMPLEMENTATION

Symplectic 3D SC Kick

We will concentrate here on the main MADX-SC design principles, further details can be found in Ref. [3].

The SC kick will be automatically symplectic if it is derived from a potential. We assume the bunch charge density to be of the form

$$\rho(x,y,z,t) = \frac{\lambda(z-v_0 t)}{2\pi\sigma_x\sigma_y}\exp\left(-\frac{x^2}{2\sigma_x^2}-\frac{y^2}{2\sigma_y^2}\right), \quad (1)$$

with λ being the line charge density, which should not be necessarily Gaussian but the present implementation is limited to a Gaussian profile.

For a long bunch, $\sigma_z \gg \max(\sigma_x, \sigma_y)$, the space-charge potential can be factorized in a similar fashion

$$\phi(x,y,z,t) \cong \lambda(z-v_0 t)\cdot\Phi(x,y), \quad (2)$$

where the two-dimensional potential function Φ can be presented in the form [7] [1]

$$\Phi(x,y) = \int_0^1 \left\{\exp\left(-\frac{x^2 t}{2\sigma_x^2}-\frac{y^2 r^2 t}{2\sigma_y^2[1+(r^2-1)t]}\right)-1\right\}\frac{\mathrm{d}t}{t\sqrt{1+(r^2-1)t}}, \quad (3)$$

with $r=\frac{\sigma_y}{\sigma_x}$ for $\sigma_y<\sigma_x$. If $\sigma_y>\sigma_x$ one can use formulas with interchanged x and y. Computing all components of a quasi-stationary Maxwellian field from the same potential ensures the symplecticity of the associated kick.

The potential in Eq. (3) is regularized and satisfies the boundary condition

$$\Phi(x,y)|_{x=y=0} = 0. \quad (4)$$

As a future development it can be complemented with a longitudinal wake which is independent of the transverse position (in order not to break the symplecticity).

Note [7] discusses the derivation of Eq. (3) in detail and considers methods of its numerical calculation in cases of small, large, and intermediate values of the transverse displacement, in units of beam sizes. Report [8] presents precision tests for each of these cases.

[1] Gaussian units are used. To convert to SI units the r.h.s. should be divided by $4\pi\varepsilon_0$

ISBN: 978-3-95450-225-7 ISSN: 2673-5571 doi:10.18429/JACoW-HB2021-MOP21

Ref. [3] summarizes the main results. For different transverse displacements the evaluation of the potential can be separated into three, mostly distinct regions: Power Series Expansion, Asymptotic Expansion and Numerical Integration.

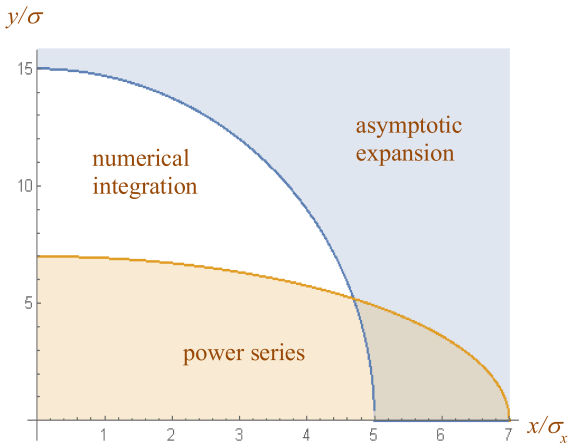

Figure 1: Regions of good precision for power series and asymptotic expansion for aspect ratio $r = \frac{\sigma_y}{\sigma_x} = \frac{1}{3}$. For coordinates in the white region the numerical integration has to be used.

In Figure 1 for the region where numerical integration is required one needs to determine the relative error in Φ vs. the number of integration steps.

Figure 2 shows the precision of the potential found using the Simpson rule as a function of the number of steps of integration. Errors in E_x and E_y are about two orders of magnitude lower.

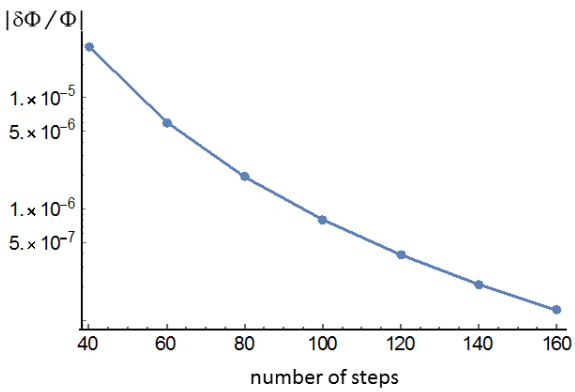

Figure 2: Relative error in Φ vs. the number of integration steps.

About 100 grid points in Fig. 2 appear to be sufficient for various cases we have studied.

Beam Sigma and Optics Calculation without Twiss

The beam sizes should be periodically updated (e.g. every turn) based on the evolving particle distribution. The previously implemented algorithm (described a posteriori in [9]) requires stable optics using the MAD-X Twiss command: first to find the action variables of the normal modes for each particle at the observation point to determine emittances; and then to calculate the beam sizes with updated emittances at all space-charge elements.

The optics functions can also be updated but, even if the stable periodic solution exists, this significantly slows down the computation.

Another drawback of the old algorithm is the rather soft suppression of the halo particles contribution to the emittance leading to larger beam sizes and weaker space-charge kicks.

A different approach was proposed in [10], which involves the exact Gaussian fit of the particle distribution in terms of the beam Σ matrix and its subsequent propagation from the observation point along the lattice using the transfer matrix T as

$$\Sigma^{(2)} = T \cdot \Sigma^{(1)} \cdot T^t, \tag{5}$$

where superscript "t" means transposition.

The precision of the fit was checked in [10] for a one-dimensional distribution. Tests with a multi-dimensional distribution revealed problems with spurious coupling, which only slowly decreases with the number of particles and in the case of equal emittances does not decrease at all.

The probable cause of the spurious coupling is the very strong suppression of the contribution of particles with even moderate amplitudes, effectively reducing the number of particles. To alleviate this problem, the fitting algorithm was modified in the way described below.

First of all, we shall show that the fitting formulas in [10] can be obtained from simple considerations valid also for other types of model distribution function. Let z_i, i=1,…, n be the n-dimensional phase space coordinates and $W(z_1,\ldots,z_n)$ some weight function that we will use for construction of the Σ matrix from a sample of N particles, while trying to approximate this sample with the model distribution function $F(z_1,\ldots,z_n)$. In what follows we will denote the n-tuple (z1, ... ,zn) by z.

Let $F(z)$ be the actual normalized beam distribution function. Then, as a consequence of the law of large numbers, we will have for any function $H(z)$ in the limit of large number of particles $N\to\infty$

$$\frac{1}{N}\sum_{k=1}^{N} H(z^{(k)}) \xrightarrow[N\to\infty]{} \int_\Omega H(z)F(z)d^n z, \tag{6}$$

with Ω being the available phase space.

Now we can define the fitted Σ matrix using weight function $W(z)$ as

$$\sum_{ij}^{(fit)} = \frac{\frac{1}{N}\sum_{k=1}^{N} z_i^{(k)} z_j^{(k)} W(z^{(k)})}{\frac{1}{N}\sum_{k=1}^{N} W(z^{(k)}) - p}, \tag{7}$$

with p being some parameter. Imposing the requirement that matrix Eq. (7) coincides with the actual Σ matrix in the limit $N\to\infty$

ISBN: 978-3-95450-225-7 ISSN: 2673-5571 doi:10.18429/JACoW-HB2021-MOP21

$$\sum_{ij}^{(exact)} = \int_\Omega z_i z_j F(z) d^n z, \tag{8}$$

we have for non-zero elements $\Sigma_{ij}^{(\mathrm{exact})}$

$$p = \int_\Omega W(z)F(z)d^n z - \frac{1}{\sum_{ij}^{(exact)}} \int_\Omega z_i z_j W(z)F(z)d^n z. \tag{9}$$

In the case of Gaussian distribution and weight functions

$$\begin{aligned} F(\underline{z}) &= \frac{1}{(2\pi)^{\frac{n}{2}}\sqrt{det\,\Sigma}} \exp[-\tfrac{1}{2}(\underline{\zeta}, \Sigma^{-1}\underline{\zeta})], \\ W(\underline{z}) &= \exp[-\alpha(\underline{\zeta}, \Sigma^{-1}\underline{\zeta})], \end{aligned} \tag{10}$$

where ζ are n-dimensional vectors of displacements from some average values, we obtain

$$p = \frac{2\alpha}{(1+2\alpha)^{\frac{n}{2}+1}}. \tag{11}$$

With $\alpha = 0, p = 0$ Eq. (7) provides simple r.m.s. values while with $\alpha = \frac{1}{2}, p = \frac{1}{2^{\frac{n}{2}+1}}$ we retrieve the result of [10]. By adjusting α we can suppress the contribution of halo particles while not cutting into the beam core. The choice $\alpha = \frac{1}{4}$ greatly reduced the spurious coupling. It should be noted that with $\alpha \neq \frac{1}{2}$ this fit does not render the minimum of the integrated squared difference in the phase density of actual particle distribution and the model distribution in this sense is not exact. However, it leads to more practical results.

Since the Σ matrix is not known, Eq. (7) is a non-linear equation which can be solved iteratively. The full set of equations to solve is:

$$\underline{a} = \frac{\sum_{k=1}^N \underline{z}^{(k)} \exp[-\alpha(\underline{\zeta}^{(k)}, \Sigma^{-1}\underline{\zeta}^{(k)})]}{\sum_{k=1}^N \exp[-\alpha(\underline{\zeta}^{(k)}, \Sigma^{-1}\underline{\zeta}^{(k)})]}, \quad \underline{\zeta}^{(k)} = \underline{z}^{(k)} - \underline{a}, \tag{12}$$

$$\sum_{ij} = \frac{\frac{1}{N}\sum_{k=1}^N \zeta_i^{(k)}\zeta_j^{(k)} \exp[-\alpha(\underline{\zeta}^{(k)}, \Sigma^{-1}\underline{\zeta}^{(k)})]}{\frac{1}{N}\sum_{k=1}^N \exp[-\alpha(\underline{\zeta}^{(k)}, \Sigma^{-1}\underline{\zeta}^{(k)})] - \frac{2\alpha}{(1+2\alpha)^{\frac{n}{2}+1}}}. \tag{13}$$

The iterative procedure for Eqs. 12 and 13 has a tendency to overshoot, but the convergence can be improved by the introduction of a damping factor $0 < d < 1$:

$$\Sigma_l = d\Sigma_l^{(formula)} + (1-d)\Sigma_{l-1}, \tag{14}$$

where l is the iteration number. Tests showed that d =0.85 is close to the optimum.

The Σ matrix propagated along the lattice according to Eq. (5) may contain a free-oscillating part due to e.g. initial mismatch. This gives us the ability to study the effects of interaction of individual particles with coherent (envelope) oscillations, such as halo formation [11] and Landau damping.

With a finite number of macro-particles there are inevitable statistical fluctuations which act as a never ending pump, increasing beam emittance through this interaction. The obvious remedy, a larger number of macro-particles, defeats our goal of the speed of simulations.

Thus we have to consider two modes of operations: freely propagating Σ and periodic Σ. The first option allows one to study envelope resonances but requires the maximum available number of particles to suppress the statistical noise. The second option is analogous to the existing MAD-X algorithm but more efficiently suppresses the halo contribution to emittances and includes effects of the machine coupling (we plan to add coupling through the space charge forces in the future).

The periodic Σ option requires the existence of a stable optics and it involves computation of the eigen-mode emittances ε_m, m=1,2,3, which are imaginary parts of eigenvalues of matrix

$$\Omega = S, \tag{15}$$

with S being the symplectic unity matrix

$$S = \begin{pmatrix} 0 & 1 \\ -1 & 0 \end{pmatrix} \oplus \begin{pmatrix} 0 & 1 \\ -1 & 0 \end{pmatrix} \oplus \begin{pmatrix} 0 & 1 \\ -1 & 0 \end{pmatrix}. \tag{16}$$

After completing turn n-1, we obtain the transfer matrix T(n-1) and the particle distribution at the starting point of turn n. We use the algorithm as calculated above for $\Sigma(n)$ but instead of propagating it around machine we use it for computing normal mode emittances ε_m from matrix Eq. (15). To build a (quasi-) periodic $\widetilde{\Sigma}(n)$ at the starting point of turn n we also need the eigenvectors of the 1-turn transfer matrix that has three complex-conjugate pairs of eigenvalues and eigenvectors

$$T\underline{\nu}_k = \lambda_k \underline{\nu}_k, \ \lambda_{2m} = \lambda_{2m-1}^*, \ \underline{\nu}_{2m} = \underline{\nu}_{2m-1}^* \tag{17}$$

where m=1,2,3 is the mode number, asterisk denotes complex conjugation, underscore means 6D vector. We choose the same normalization as used in MAD:

$$(\underline{\nu}_{2m-1}^*, S\underline{\nu}_{2m-1}) = 2i, \tag{18}$$

that can be rewritten for real and imaginary parts of the eigenvectors as

$$\begin{aligned} &(\underline{\nu}'_i, S\underline{\nu}'_j) = (\underline{\nu}''_i, S\underline{\nu}''_j) = 0, \\ &(\underline{\nu}'_{2m-1}, S\underline{\nu}''_{2n-1}) = \delta_{mn}, \\ &\underline{\nu}'_i \equiv \mathrm{Re}(\underline{\nu}_i), \quad \underline{\nu}''_i \equiv \mathrm{Im}(\underline{\nu}_i). \end{aligned} \tag{19}$$

Assuming that the new transfer matrix, T(n), will not differ much from T(n-1), we can use eigenvectors of T(n-1) to build $\widetilde{\Sigma}(n)$ according to [12–14]

$$\widetilde{\Sigma}_{ik} = \sum_{m=1}^{3} \epsilon_m (\nu'_{2m-1,i}\,\nu'_{2m-1,k} + \nu''_{2m-1,i}\,\nu''_{2m-1,k}), \tag{20}$$

where $\nu_{m,k}$ means k-th component of m-th eigenvector. The eigenvectors can be propagated around the ring for Eq. (20) to be applied at every space-charge kick. Alternatively, $\widetilde{\Sigma}(n)$ can be propagated around the ring using MAD-X sectormaps.

ISBN: 978-3-95450-225-7 ISSN: 2673-5571 doi:10.18429/JACoW-HB2021-MOP21

SC Simulations Predictions

In 2012 a dedicated PS experiment was conducted to study beam stability and emittance blow-up due to SC and sextupole non-linearities. Table 1 shows the relevant parameters from this experiment. The results were published in 2017 [15].

Table 1: Beam Characteristics for the 2012 PS Experiment

Parameter	Value
Intensity [1×10^{10} ppb]	55
Bunch length (rms) [m]	9.59
$\Delta p/p$ (rms) [10^{-3}]	0.95
ε_x^n (1σ) [μm]	3.5
ε_y^n (1σ) [μm]	2.2
Turns in Machine/Simulations	500,000

Using the beam parameters from the 2012 experiment, a first test was done to study the impact of the number of macro-particles on the resulting artificial emittance growth in the simulations. Figure 3 shows that for the PS the turn-by-turn "noise" of the obtained emittance values goes down by roughly a factor of two, which might be expected when raising the number of macro-particles by a factor of four. The long-term blow-up is also largely reduced. The "apparent"reduction of emittance at the beginning seems to be an artifact of the very small number of macro-particles used in the simulations. In the following we have used 2,000 macro-particles, i.e. by a factor 2 more than in the original simulations. Fortunately, we took advantage of the factor of 2 in speed-up due to optimization, but we still need some 4 weeks of CPU on CERN's PC farms for each run.

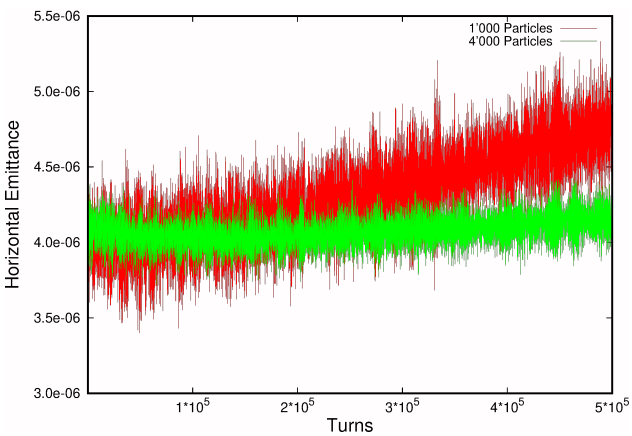

Figure 3: Horizontal emittance evolution versus turn number for the CERN PS for 1,000 and 4,000 macro-particles respectively. Both turn-by-turn noise and long-term emittance growth due to numerical noise decrease with the number of macro-particles, the former by a factor of 2.

The following Figures 4 to 7 show the comparison of the PS experiments with predictions of simulations of a recent MADX-SC version: Fig. 4 shows the horizontal distributions at the start; Fig. 5 the horizontal distributions after 500,000 turns; Fig. 6 the vertical distributions at start, and Fig. 7 the vertical distributions after 500,000 turns.

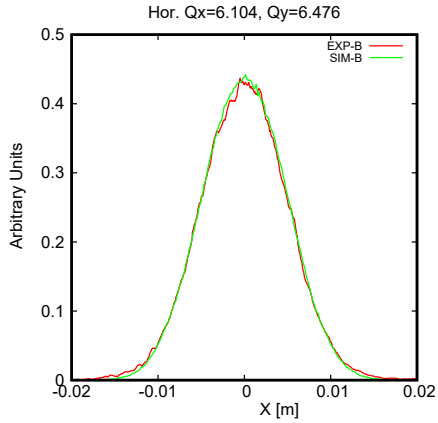

Figure 4: Horizontal Distribution at start, the experimental data are in red, the simulations in green.

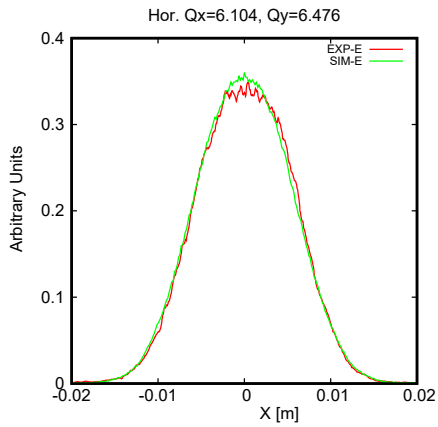

Figure 5: Horizontal Distribution after 500,000 turns, the experimental data are in red, the simulations in green.

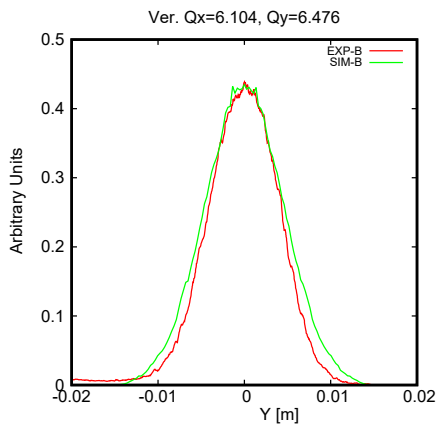

Figure 6: Vertical Distribution at start, the experimental data are in red, the simulations in green.

The two main features of agreement with the experiment are the facts that the broadening of the horizontal profile

ISBN: 978-3-95450-225-7 ISSN: 2673-5571 doi:10.18429/JACoW-HB2021-MOP21

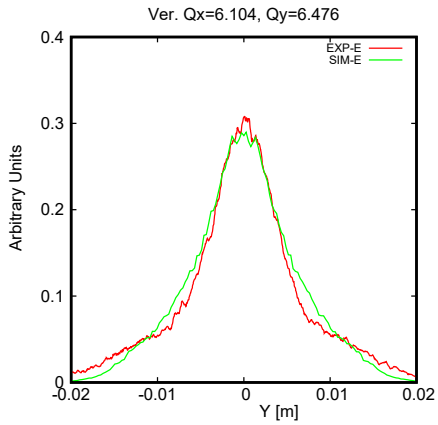

Figure 7: Vertical Distribution after 500,000 turns, the experimental data are in red, the simulations in green.

is well reproduced and the development of vertical tails is almost perfectly followed. Moreover, the obtained results are in very good agreement with previous simulation results reported in [15].

PORTING TO LATEST MAD-X VERSION

The SC calculation described in this paper was first implemented in the test version of MAD-X at FNAL. In recent years, the official CERN MAD-X version of the code has undergone significant restructuring and consolidation. Among various interventions, the original Fortran 77 code has been partially rewritten to benefit from the latest features offered by the Fortran 90 language. Matrix operations, for instance, that were originally performed with dedicated subroutines have been rewritten to use the native matrix operators provided by F90. In this framework, the SC routines have also been restructured before being updated to include the latest new features introduced in the FNAL test MAD-X version, described in this paper.

A new module was created, containing all the SC- / beam-beam-related routines that in the FNAL MAD-X version were originally hard-coded in the modules TWISS and TRACK. The new space-charge module was provided with a simple interface, consisting of just three functions: Initialize, Update, and Finalize the SC kick, which are directly called from TWISS and TRACK. This restructuring allowed us to improve the overall readability and maintainability of the code, while enabling dedicated optimizations.

Subsequently, the latest features of the SC calculation, described in this paper were introduced, and a work of optimization was carried out to benefit from multi-core parallelism, through OpenMP. A fine tuning of the code and dedicated benchmarks allowed us to optimize the overall performance of the simulation. The work of integrating the new SC routines in the latest official version of MAD-X is being completed, and we expect it to be available from the next MAD-X release, 5.08.00.

Another important issue is the set-up phase that simplifies the lattice, introduces SC kicks in a controlled way and the adiabatic switching on of the SC kick strength to minimize the problem of unstable optics detected with TWISS, i.e. the attempt to approach the tune working-point as close as possible to integer or half-integer resonances. In the original coding all these tasks were performed with MAD-X macros. This is quite alright concerning the results but for any new user it was exceedingly difficult to adapt a new case to this structure. During the Fermilab visit in 2012 a large number of macros were turned into MAD-X code. Nevertheless, a 3-step expert set-up procedure was still needed for any new case. In 2021, and in conjunction with an upgrade of the manual, we automated these steps in a way such that a typical MAD-X user should now be able to operate the code just with the use of this manual. A bit of fine-tuning is still in progress.

CONCLUSIONS

This paper summarized the development of the MADX-SC Fermilab code in a collaboration between FNAL and CERN finalized at the end of 2018. In the meantime the code has evolved, as the result of an intense debug and optimization work. In particular, a speed-up of a factor of 2 has been accomplished. The simulation results presented in this paper have been obtained using a more recent version of the code. In parallel, there has been a significant effort to port all changes to the latest MAD-X version. The set-up phase has been simplified and the manual is being updated.

We still have a significant program to extend the scope of the code. In particular, to allow for distributions beyond Gaussian.

REFERENCES

[1] V. V. Kapin and Y. Alexahin, "Space Charge Simulation Using MADX with Account of Synchrotron Oscillations", in *Proc. 22nd Russian Particle Accelerator Conf. (RuPAC'10)*, Protvino, Russia, Sep.-Oct. 2010, paper WEPSB017, pp. 204–206.

[2] T. Persson, L. Deniau, and G. Roy, "The madx program (methodical accelerator design), version 5.07.00,", May 2021. http://cern.ch/madx/releases/5.07.00/madxuguide.pdf

[3] F. Schmidt and Y. Alexahin, "New SC Algorithm for MAD-X," Oct. 2018, Revised Nov. 2019. https://cds.cern.ch/record/2644660

[4] V. Kapin, A. Latina, H. Renshall, and F. Schmidt, "MADX-SC Flag Description" to be published.

[5] C. Montag, private communication, Apr. 2014.

[6] J. Ostiguy and J. Holmes, "PyORBIT: A Python Shell for ORBIT", in *Proc. 20th Particle Accelerator Conf. (PAC'03)*, Portland, OR, USA, May 2003, paper FPAG018, p. 3503.

ISBN: 978-3-95450-225-7 ISSN: 2673-5571 doi:10.18429/JACoW-HB2021-MOP21

[7] Y. Alexahin, "New Formulae for 3DoF Space Charge Field," FNAL, Batavia, IL, USA, FNAL Beams-doc-5032-v3, 2017.

[8] Y. Alexahin, "Progress on 3D space charge kick," Batavia, IL60510, USA, Mar 2018. https://indico.cern.ch/event/688897

[9] Y. Alexahin, V. Kapin, F. Schmidt, A. Valishev, and R. Wasef, "Adaptive Space Charge Calculations in MADX-SC", in *Proc. North American Particle Accelerator Conf. (NAPAC'16)*, Chicago, IL, USA, Oct. 2016, pp. 1126–1128. doi:10.18429/JACoW-NAPAC2016-THPOA15

[10] Y. Alexahin, "Computing Eigen-Emittances from Tracking Data", in *Proc. North American Particle Accelerator Conf. (NAPAC'16)*, Chicago, IL, USA, Oct. 2016, pp. 1132–1134. doi:10.18429/JACoW-NAPAC2016-THPOA17

[11] R. L. Gluckstern, "Analytic model for halo formation in high current ion linacs," *Phys. Rev. Lett.*, vol. 73, pp. 1247–1250, Aug. 1994. doi:10.1103/PhysRevLett.73.1247

[12] G. Ripken, "Investigations on disturbances in the storage ring caused by the detector field and their corrections (in German),", DESY, Hamburg, Germany, DESY-R-1-70/5, Jun. 1970.

[13] L. H. A. Leunissen, F. Schmidt, and G. Ripken, "Six-dimensional beam-beam kick including coupled motion," *Phys. Rev. ST Accel. Beams*, vol. 3, p. 124002, Dec. 2000. doi:10.1103/PhysRevSTAB.3.124002

[14] C. Iselin, "The MAD program (methodical accelerator design), version 8.13, physical methods manual," May 1992.

[15] G. Franchetti, S. Gilardoni, A. Huschauer, F. Schmidt, and R. Wasef, "Space charge effects on the third order coupled resonance," *Phys. Rev. Accel. Beams*, vol. 20, p. 081006, Aug 2017. doi:10.1103/PhysRevAccelBeams.20.081006